Article

Not peer-reviewed version

Spin Label Electron Paramagnetic Resonance Spectroscopy Reveals Effects of Wastewater Filter Membrane Coated with Titanium-Dioxide Nanoparticles on Bovine Serum Albumin

Krisztina Sebők-Nagy , Zoltán Kóta , András Kincses , Ákos Ferenc Fazekas , András Dér , Zsuzsanna László , Tibor Páli *

Posted Date: 15 August 2023

doi: 10.20944/preprints202308.1111.v1

Keywords: wastewater cleaning; polyvinylidene fluoride filter membrane; titanium-dioxide nano-particles; P25; serum albumin; spin label EPR; fluorescence; dynamic light scattering

Article

Spin Label Electron Paramagnetic Resonance Spectroscopy Reveals Effects of Wastewater Filter Membrane Coated with Titanium-Dioxide Nanoparticles on Bovine Serum Albumin

Krisztina Sebők-Nagy [1], Zoltán Kóta [1], András Kincses [1], Ákos Ferenc Fazekas [2], András Dér [1], Zsuzsanna László [2] and Tibor Páli [1,*]

[1] Institute of Biophysics, Biological Research Centre Szeged, Szeged, Hungary; seboknagy.krisztina@brc.hu (K.S.-N.); kota.zoltan@brc.hu (Z.K.); kincses.andras@brc.hu (A.K.); der.andras@brc.hu (A.D.)

[2] Department of Biosystems Engineering, Faculty of Engineering, University of Szeged, Szeged, Hungary; fazekas@mk.u-szeged.hu (Á.F.F.); zsizsu@mk.u-szeged.hu (Z.L.)

* Correspondence: pali.tibor@brc.hu

Abstract: Accumulation of proteins in filter membranes limits the efficiently of filtering technologies for cleaning wastewater. Efforts are ongoing to coat commercial filters with different materials (such as titanium-dioxide, TiO_2) in order to reduce the fouling of the membrane. Beyond monitoring the desired effect of retention of biomolecules, it is demanding to understand what are the biophysical changes in water-soluble proteins caused by interacting with the new coated filter membranes, an aspect that has received little attention so far. Using spin label electron paramagnetic resonance (EPR), aided with native fluorescent spectroscopy and dynamic light scattering (DLS), here we report the changes in the structure and dynamics of bovine serum albumin (BSA) exposed to TiO_2 (P25) nanoparticles or passing through commercial polyvinylidene fluoride (PVDF) membranes coated with the same nanoparticles. We have found that the filtering process and prolongued exposure to TiO_2 nanoparticles had significant effects on different regions of BSA, and denaturation of the protein was not observed, neither with TiO_2 nanoparticles nor by pressing through TiO_2-coated filter membranes.

Keywords: wastewater cleaning; polyvinylidene fluoride filter membrane; titanium-dioxide nano-particles; P25; serum albumin; spin label EPR; fluorescence; dynamic light scattering

1. Introduction

The efficiency of filtering of biomolecules certainly depends on the effect of the surface of the filter on the biomolecules. Separation of proteins from aqueous solutions can be efficiently achieved by membrane filtration. However, the membrane fouling seriously limits its application when proteins tend to adsorb to the surface of the membrane pores, hence reducing the pass-through efficiency and ultimately the lifespan of the membranes. An ideal filter membrane would keep proteins in the pre-filter space without loosing its filtering efficiency. Until now, several new methods were developed to produce antifouling membranes, such as membrane modification by nanoparticles (e.g. titanium-dioxide, TiO2). Although a number of modified membranes were developed, there is only limited information available regarding whether the applied nanoparticles cause any changes in protein structure, altering their filterability and other biophysical properties [1–3]. Our previous results showed that coating membranes with TiO2 surprisingly worsened the retention of bovine serum albumin (BSA) [4,5]. This phenomenon can only be partially explained by changes in the roughness and morphology of the membrane surface, and previous investigations have also raised the possibility of the changes of protein structure as well [6]. In the present study we address precisely this aspect of filtering out proteins from wastewater. We have chosen BSA as the model protein in this work not only because

Preprints (www.preprints.org) | NOT PEER-REVIEWED | Posted: 15 August 2023 doi:10.20944/preprints202308.1111.v1

other teams [7–11] and we also have used it in our recent relevant studies [4,5,12] but also because it is a well known protein with plenty of biophysical data about its water-soluble state [13–18] that can serve as reference for comparison. Spin label EPR spectroscopy is our main technique here because it has proven to be among the most powerful techniques in studying serum albumins [19–22]. Commercial PVDF filter membranes were modified by coating them with TiO2 nanoparticles (P25), and the effects of filtration through neat (un-coated) and TiO2-coated membranes and contact with TiO2 on protein structure were investigated by spin label EPR and native fluorescence spectroscopy as well as DLS to reveal the potential changes in the protein structure.

Apart from diverse physiological functions, serum albumins are the major vehicles of fatty acid transport through blood plasma, as they can bind several long-chain fatty acids with high affinity [23–26]. Due to this fatty acid binding function of BSA [27–31] and because spin label EPR spectroscopy played a crucial role in identifying and characterising the fatty acid binding sites of serum albumins [27,30–33], we have used a spin-labelled stearic acid analogue (5-SASL) to detect changes in the fatty acid binding of the protein in its process-relevant interactions with the membrane and the nanoparticles. Fatty acid binding to serum albumins has proven to be sensitive to the physical state of the protein (affected by, e.g., pH, ligand-induced allosteric modulation, temperature) [25,27,28,32]. We have also used two common maleimide-type spin labels binding to un-blocked Cys residues in order to detect changes in the dynamics of the spin-labelled Cysteines and structural changes in their vicinity [21,34–37]. According to the crystal structure [38] the labelled residue is likely to be Cys34 (Figure 1. blue coloured residue in sequence and structure [39,40]) because the others are participating in disulfide bridges [21,28].

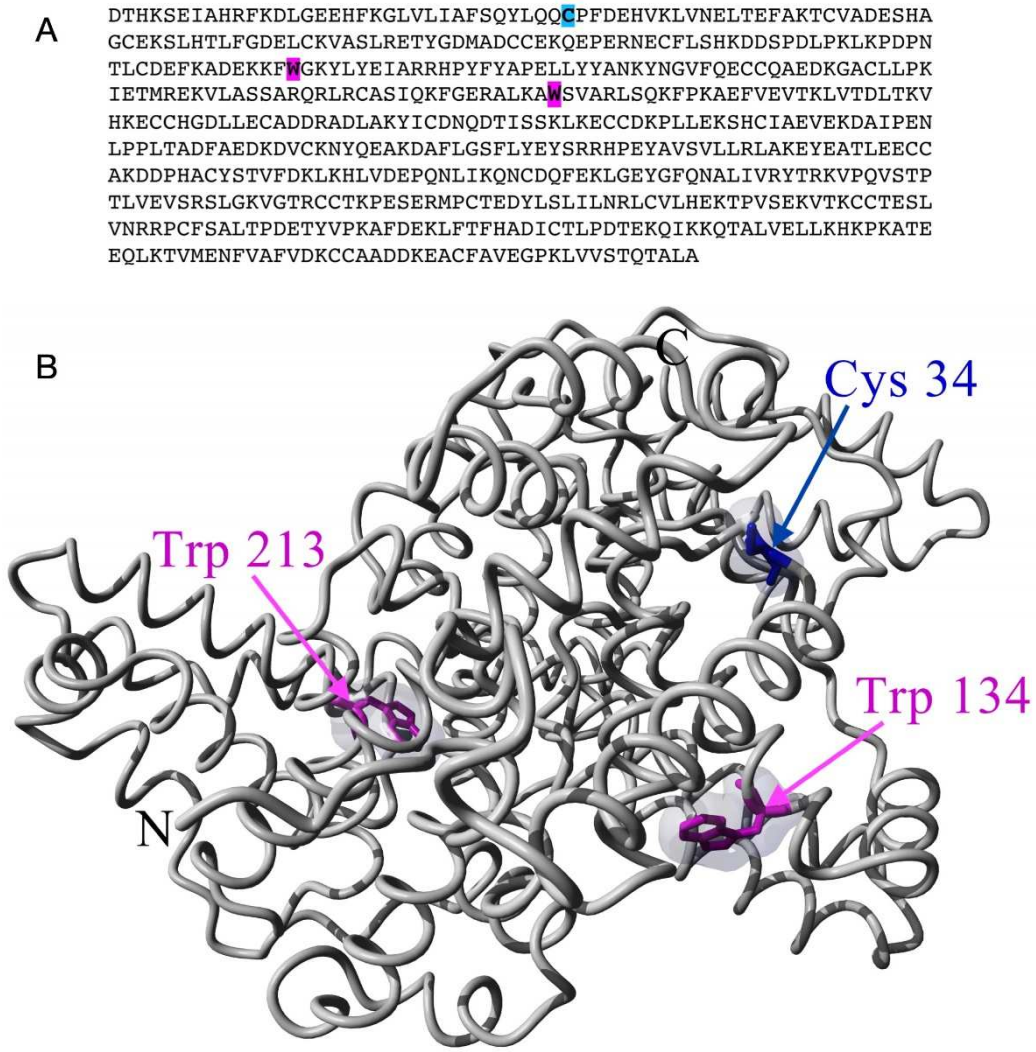

 doi:10.20944/preprints202308.1111.v1

Figure 1. The amino acid sequence (**A**) and an illustrative 3-dimensional structure (**B**) of BSA (4s5f). The autofluorescence residues (W, Trp) and the spin label biding site (C, Cys) are highlighted and coloured in magenta and blue, respectively.

The fluorescent residues in BSA offer a label-free technique via autofluorescence [41–43]. Indeed, the 2 Tryptophan residues of BSA (Figure 1, magenta coloured) are sensitive to conformational changes via altered polarity and rotational dynamics [42–45]. Therefore we have carried out fluorescence spectroscopic measurements for BSA, BSA exposed to TiO_2 nanoparticles and for filtered BSA. Since BSA maybe present in different states in an aqueous solution depending on its concentration and other conditions, such as folded or denatured monomeric, multimeric aggregated and micellar forms [10,14,22,46], we tested changes in the particle size distribution of BSA upon the above different treatments using dynamic light scattering (DLS).

2. Results and Discussion

2.1. Chemical oxygen demand (COD)

The BSA rejection of the pristine and modified membranes in the presence (BSA@PVDF/TiO2) or absence of TiO2 (BSA@PVDF) are illustrated in Table 1.

Table 1. BSA retention during filtration of BSA through PVDF or PVDF/TiO_2 composite membrane.

Solution	c(BSA), (g/L)	Membrane	R%
BSA	1	PVDF	92
BSA	1	PVDF/TiO_2	28
BSA(TiO_2)	1	PVDF	91
BSA(TiO_2)	0.33	PVDF	37
BSA	0.33	PVDF	37

It was found that the pristine membrane rejects more BSA than the modified one. This is a very surprising result; thus it was also checked if the higher BSA permeability of the membrane caused by the contact of BSA with TiO_2 nanoparticles. The BSA was mixed with TiO_2 then the BSA was separated from TiO_2 by microfiltration, and the clean BSA solution was filtered through the PVDF membrane (BSA(TiO_2)@PVDF). It was found, that the contact of BSA with TiO_1 had no noticable change the filtration performance after separated from TiO_2. The filtration alone through CA membrane caused approx. 5% BSA loss from 1 g/L solution, while the retention during filtration through PVDF membrane was dependent on BSA concentration; in 3 fold diluted solutions the retention decreases. Nevertheless, this cannot explain the decreased retention of BSA filtered through the TiO_2 modified membrane, thus in further experiments the potential effect of the contact of TiO_2 and BSA on BSA structure was investigated.

2.2. Dynamic light scattering (DLS)

We tested the particle size distribution of BSA in our samples with dynamic light scattering (DLS). Table 2 summarises our data along with the different states of BSA in aqueous environment. The DLS curves for the stock (60 μM) and the 100-fold diluted BSA solution can be seen in Figure 2.

Preprints (www.preprints.org) | NOT PEER-REVIEWED | Posted: 15 August 2023 doi:10.20944/preprints202308.1111.v1

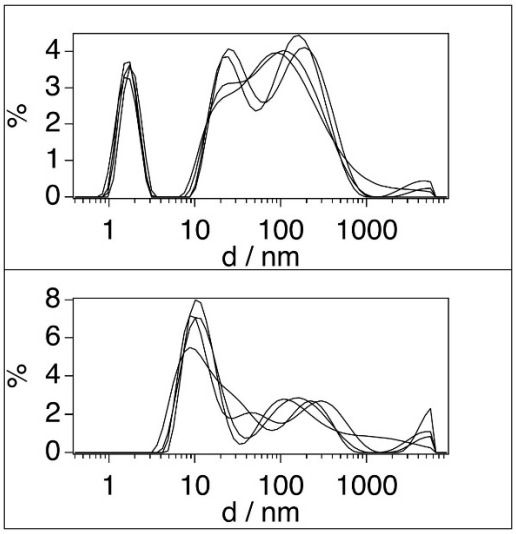

Figure 2. Particle size distribution in BSA solutions in water, [BSA]=6x10^{-5} M (top), [BSA]=6x10^{-7} M (bottom). The different curves represent independent experiments.

A prominent narrow peak at around a mean particle sizes of 1.7 nm, and two very broad and highly overlapping peaks at 24.4 and 85-102 or 105-200 nm are present in the BSA stock solutions (Figure 2, top). The 100-fold diluted BSA solution (Figure 2, bottom) results in the disappearance of the peaks at 1.7 nm and the appearance of a new peak at ~11 nm can be observed along with the strong reduction of the broad (20-1000 nm) scattering region. There are a wide range of particle sizes reported for BSA in different concentration regions and conditions as summarised in Table 2.

Table 2. Particle size of BSA.

[BSA]/μM	d1/nm	d2/nm	Particle type	Medium	Reference
0.6		11	small micelles or other forms of aggregates (d2)	H_2O	own result
0.65		8.9	compact aggregates (d2)	pH 7.2, 10 mM phosphate buffer	[16]
4.5	10		monomer (d1)	pH 7.0, H_2O	[17]
5	7.3	13.5	monomer (d1), dimer (d2)	pH 7.4, H_2O	[46]
10	3.4		monomer (d1)	pH 7.0, H_2O	[18]
25		10.6	compact aggregates (d2)	pH 7.2, 10 mM phosphate buffer	[16]
60.2	1.7	22	small micelles (d1) large aggregates (d2)	H_2O	own result
100	5.2		undefined particle (d1)	pH 7.4, H_20	[47]
120.4	2	22	denaturated monomers (d1), aggregation of denaturated monomers (d2)	H_2O	[48]

Comparing our results with this set of previously reported data, we can conclude that the 11 nm peak in our 100-fold diluted solution is likely to correspond to small micelles or other forms of aggregates, whereas the non-diluted BSA dispersion contains large aggregates and a minor contribution of small micelles. It is important to note, that in the present work the concentration of BSA was 10 or 100 times higher (for the diluted and the stock solutions, respectively) than the 0.65-0.69 μM critical micelle concentration (CMC) [16]. Therefore disappearance or dissolution of micelles upon filtering and interaction with TiO_2 can be excluded. It should be noted here, that the average size of the membrane pore was estimated ~14 nm by Howe and Clark [49], whereas the size of the

Preprints (www.preprints.org) | NOT PEER-REVIEWED | Posted: 15 August 2023 doi:10.20944/preprints202308.1111.v1

primer TiO_2 particles is ~25.4 nm, but they form aggregates in water with a diameter of ~1 μm [50]. It is therefore a very low probability for the TiO_2 particles to pass through the membrane pores, consequently TiO_2 content must be negligible in the filtered BSA sample.

2.3. Fluorescence spectroscopy

BSA has two Tryptophan residues (Trp134 and Trp213, see Figure 1) with fluorescence emission maxima at ~348 nm in pure water [51]. Fluorescence from the Tyrosines is negligible compared to that of Tryptophanes [42]. We have made fluorescence spectroscopic measurements for BSA, BSA+TiO2 and filtered BSA from their stocks. Table 3 contains the wavelengths of their fitted emission maximum by Gauss function (λmax) and (weighted) mean fluorescence emission maximum (<λF>) as calculated by (Equation (1)) [52])

$$\lambda_F = \frac{\sum f_\lambda \cdot \lambda}{\sum f_\lambda} \quad (1)$$

where λ is the wavelength and f_λ is the emission intensity at λ.

Table 3. Tryptophan emission maxima.

Sample	[BSA]/M	Fitted emission maximum (λ_{max})/nm	Mean emission maximum (<λ_F>)/nm
BSA in water	$6x10^{-5}$	338.9	352.3
Filtered BSA	$1.2x10^{-5}$	340.2	356.9
BSA+TiO_2	$6x10^{-5}$	-	-
BSA in water	2x10-6	338.4	352.3
Filtered BSA	$5x10^{-7}$	340.7	355.0
BSA+TiO_2	$2x10^{-6}$	355.6	363.3

The emission maximum (λmax) and the mean emission maximum (<λF>) for the filtered sample were 340.2 nm and 356.9 nm, respectively which are red-shifted by 1.3 nm and 4.6 nm, respectively, relative to BSA sample (with λmax = 338.9, <λF>= 352.3 nm). The sample of BSA mixed with TiO2 could not be measured at this concentration because of strong light scattering. Therefore, these samples were diluted 30-fold in order to reduce the disturbing light scattering (Figure 3). Dilution alone resulted in negligible blue shift (0.5 nm) for BSA and red shift (0.5 nm) for the filtered BSA samples relatively to the original samples in case of fitted emission maximum. The mean emission maximum showed little blue shift (1.9 nm) for the filtered BSA. The diluted BSA+TiO2 sample yielded an intensity maximum at 355.6 nm (<λF>=363.3 nm), which means a strong red shift relative to BSA and filtered BSA (Figure 3, Table 3).

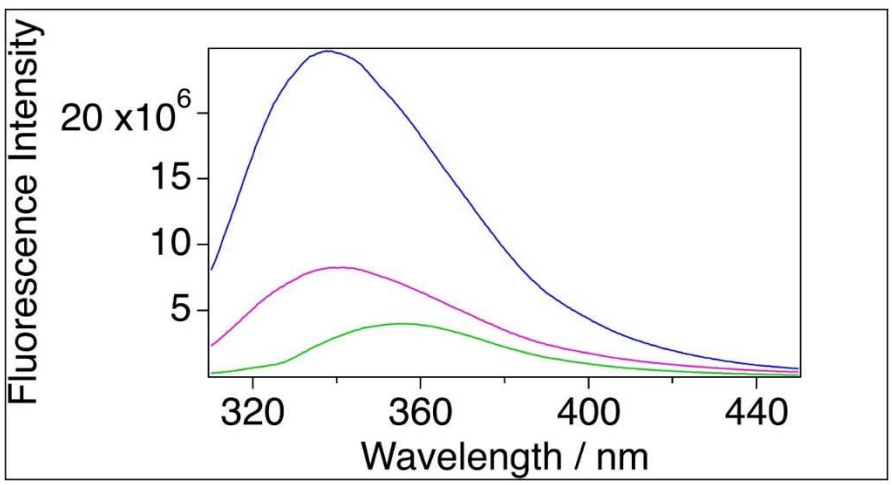

Preprints (www.preprints.org) | NOT PEER-REVIEWED | Posted: 15 August 2023 doi:10.20944/preprints202308.1111.v1

Figure 3. Representative fluorescence spectra. Blue: BSA in water ([BSA]=2x10^{-6} M), magenta: filtered BSA ([BSA]=5x10^{-7} M), green: BSA+TiO_2 ([BSA]= 2x10^{-6} M).

In case of tryptophan, any negative charge in the environment of the pyrrole ring or any positive charge close to the benzene ring causes a change in the electron densities of both rings [44], hence a bathochromic shift in the fluorescence spectrum. Based on quantum mechanics (DFT) calculations on TiO_2 it has been reported that the charge state of Ti is +3 and the oxygen is -1.5 in the molecule [53]. This means that TiO_2 is very polar and able to induce change of electron density both in the benzene and pyrrol rings. It should be noted that whereas the red-shift caused by the filtering is modest and comparable to dilution effects, that caused by direct interaction with TiO_2 is much larger. It can therefore be assumed that the observed large red shift in the spectrum of BSA+TiO_2 sample is caused by the TiO_2 molecules surrounding both the pyrrol and benzene rings. The relatively small difference between the emission maxima of BSA and filtered sample can be explained by that small amount of TiO_2 gets in the waste during the filtration.

2.4. EPR spectroscopy

The shape of the continuous wave (CW) EPR spectrum of spin labels attached to biological molecules is directly sensitive to the speed, amplitude and symmetry of the rotational dynamics of the label constrained by the orienting potential of its environment [54–57]. We have utilised both known types of labelling targets in BSA: fatty acid bound to the protein [27] and Cys residues with free sulfhydryl group [21,37]. We have used 5-SASL as a spin-labelled stearic acid analogue and 5-MSL and MTSL as covalent labels of Cys residues. These spin labels are shown in Figure 4.

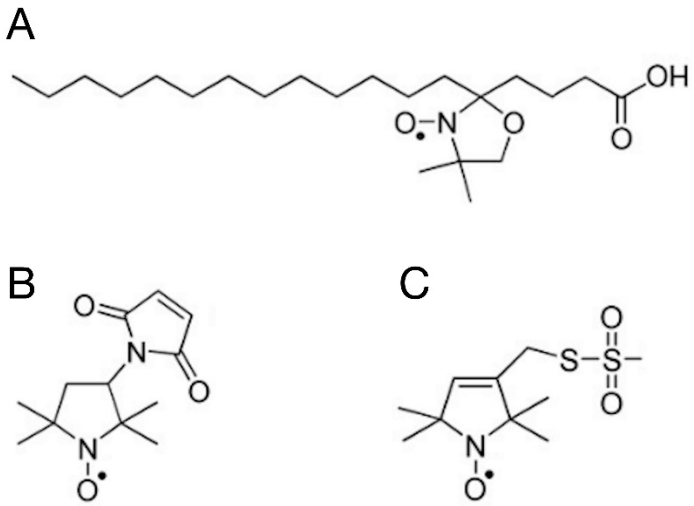

Figure 4. The chemical structure of the spin labels used for the EPR measurements. The EPR spectrum is originating from the unpaired electron located in a π* orbital of the N-O bound. (**A**): 5-SASL, (**B**): 5-MSL, (**C**): MTSL.

All three labels have some solubility in water, therefore we recorded their spectra also in the absence of BSA in order to be able to identify different spectral components in the protein-labelled samples.

2.4.1. Spin-labelling with 5-SASL

Figure 5 shows the CW EPR spectra of 5-SASL in water and in the three different aquoues samples, i.e., in BSA, filtered BSA and BSA+TiO_2.

Preprints (www.preprints.org) | NOT PEER-REVIEWED | Posted: 15 August 2023 doi:10.20944/preprints202308.1111.v1

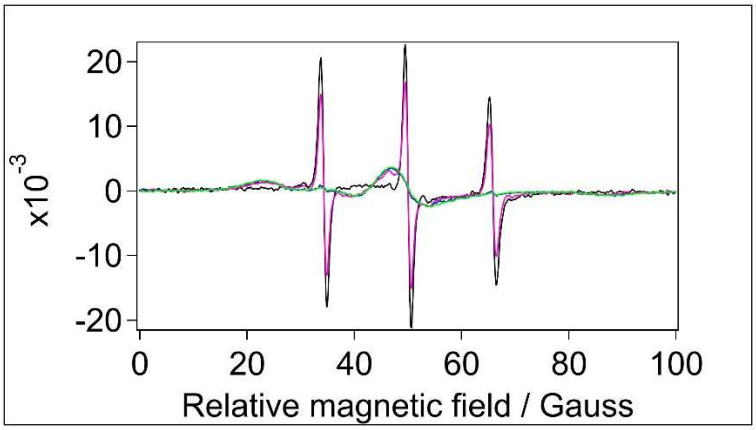

Figure 5. Normalised CW EPR spectra of samples labelled with 5-SASL. Black: water, blue: BSA in water, magenta: filtered BSA, green: BSA+TiO_2. [5-SASL]=1.2x10^{-4} M.

The spectra are normalised to the same integrated intensity (second integral), so they represent the same number of spins. 5-SASL in water has a single component EPR spectrum of three sharp lines as expected for spin label freely rotation in a solvent (see, e.g., [30]). The protein-containing samples are qualitatively similar to previous EPR reports on spin-labelled fatty acids in the presence of serum albumins [20,27,28,30,33] showing composite spectra with different contributions from a mobile and an immobile component. Since the mobile component was identical with that of 5-SASL in water, optimised subtraction allowed us to determine the shape and relative contribution of the specrtum from 5-SASL bound to BSA, and also the mobile component (see [58] for the technique). In the spectrum of the filtered BSA the mobile component is the dominant one (providing ~ 2/3 of the integrated intensity). On the contrary, the spectra of BSA and BSA+TiO2 have almost only the immobile component (with only a few percentages of mobile component). The relative contributions of the mobile and immobile components are given in Table 4.

Table 4. EPR parameters of samples spin-labelled with 5-SASL. [5-SASL]=1.2x10^{-4} M.

Sample	Mobile component/%	Immobile component/%	τ/ns	$2A_{zz}$/G
water	100	-	0.12062	-
BSA	2.4	97.6	-	64.62
Filtered BSA	71	29	0.13124	62.3-64.1
BSA+TiO_2	1.0	99.0	-	65.05

With the exception for the filtered BSA sample, the 5-SASL spectra are dominated by either the mobile or the immobile component to an extent that the "other" component is too weak for meaningful component separation. The mobile and immobile spectral shapes require different spectrum analysis to gain data on the rotational dynamics of the doxyl group of 5-SASL: The sharp hyperfine lines of the mobile component (dominating spectra of BSA in water and filtered BSA) can be used to derive the mean rotation correlation time using the Kivelson formula (Equation (2)) [59,60].

$$\tau_R(ns) = 0.65 \cdot W_0(Gauss) \cdot \left(\sqrt{\frac{h_0}{h_{-1}}} - \sqrt{\frac{h_0}{h_{+1}}} \right) \quad (2)$$

where τR is the rotation correlation time in ns, W0 is the line width of the narrowest (central) peak and h+1, h0, h-1 are the intensities of hyperfine lines. On the other hand, if the rotational dynamics is slow (on the EPR time window) or limited in amplitude then the EPR spectrum shows an anisotropic spread between the line positions at the minimum and maximum hyperfine splitting values, corresponding the z-axis of the doxyl group being oriented perpendicular or parallel, respectively, to the magnetic field. In our experiments, the immobile components represent rotational dynamics constrained by the local environment of the spin label. In this case, the orientational order determines

Preprints (www.preprints.org) | NOT PEER-REVIEWED | Posted: 15 August 2023 doi:10.20944/preprints202308.1111.v1

the inner and outer hyperfine splitting (Azz), from which orientational order parameter can usually be determined (see, e.g., [60,61]). However, the immobile components do not sufficiently expose the inner splittings and only the outer splitting constant can be easily determined (which is the half of magnetic field difference between the first local maximum and last local minimum), which are still in a monotonic relationship with the order parameter – larger outer splitting meaning higher order. The rotation correlation times and outer hyperfine splitting constants are also reported in Table 4. The rotation is very fast for water and for the filtered BSA and values (0.12062 ns and 0.13124 ns, respectively) are very close to each other, meaning that the mobile component in the filtered BSA spectrum corresponds to unbound 5-SASL. The presence of a strong immobile component in the filtered BSA and BSA+TiO2 samples suggests that the fatty acid binding site is preserved after these treatments. Similar outer splitting values (64.6 G and 65.1 G) were obtained for BSA and BSA+TiO2. The outer splitting for filtered BSA has some uncertainty because of the big signal/noise ratio of the decomposed spectrum, but it is safe to say it is ~2 G smaller for this sample. This means more disorder for 5-SASL bound to BSA mixed with TiO2, which maybe an indication of loosening the fatty acid binding pocket of BSA. The observation that in this sample the mobile component is the dominant one (responsible for more than 2/3 of the spectral intensity) is also in agreement with a perturbed binding pocket and shifted binding equlibrium.

2.4.2. Spin-labelling with 5-MSL

BSA contains 35 Cystein residues. However, according to the experimental structure of the protein (illustrated in Figure 1) and literature data, only one (Cys34) is not involved in forming S-S bridges, with a non-bonded sulfhydryl group offering a single unique site for covalent labelling with maleimide type spin labels [28,62–65]. The EPR spectra of 5-MSL added to water and the different BSA samples are shown in Figure 6 (top).

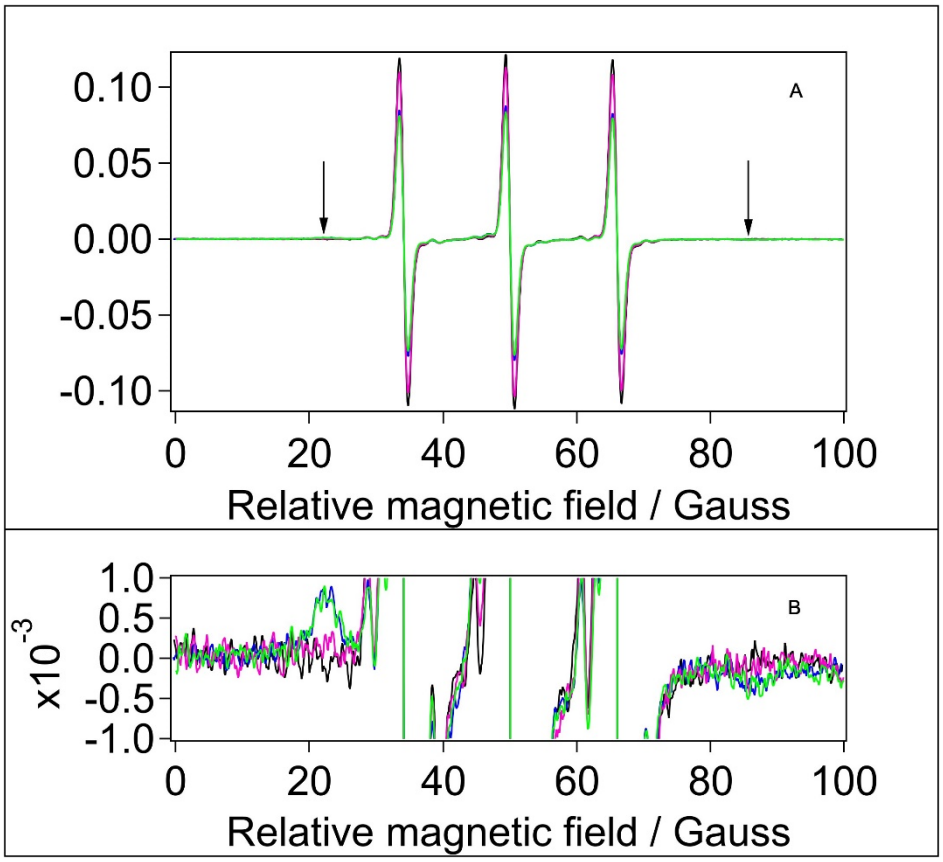

Preprints (www.preprints.org) | NOT PEER-REVIEWED | Posted: 15 August 2023 doi:10.20944/preprints202308.1111.v1

Figure 6. Normalised CW EPR spectra of samples labelled with 5-MSL. Black: water, blue: BSA in water, magenta: filtered BSA, green: BSA+TiO_2. Top: full spectra, Bottom: magnified spectrum to visualise the immobile component.[5-MSL]=$1.2x10^{-4}$ M.

According to its chemical structure (Figure 4B), covalent binding of 5-MSL to a Cystein yields a relatively rigid connection between the NO bound (bearing the unpaired electron) and the protein backbone, hence an immobile component is expected for a covalently bound 5-MSL [21,22,28,34,66]. The EPR spectra in Figure 6 (top) have very similar shapes but different intensity. (It should be kept in mind that the spectra represent the same number of spins, therefore smaller amplitudes indicate line broadening.) However, there is a clear sign of a weak immobile component present in the spectra of BSA (in water) and BSA+TiO2 (and to lesser extent in the filtered BSA) samples, as indicated by the arrows and in the bottom part of the figure. We could separate the mobile and immobile components and analyse them in a similar way as for the 5-SASL spectra, and the extracted parameters are presented in Table 5.

Table 5. EPR parameters of samples spin-labelled with 5-MSL. [5-MSL]=$1.2x10^{-4}$ M.*The immobile component of this sample is very noisy (because of its small contribution to the composite spectrum), hence the outer splitting is much less certain than for the other samples.

Sample	Mobile component/%	Immobile component/%	τ/ns	$2A_{zz}$/G
water	100	-	0.00434	-
BSA	71	29	0.00818	63.92
Filtered BSA	93	7	0.00561	cc. 61 G *
BSA+TiO2	67	33	0.00838	64.20

Comparing the corresponding immobile fractions for 5-SASL (Table 4) and 5-MSL (Table 5) it is evident that labelling of BSA is more efficient with 5-SASL than with 5-MSL. The immobile fraction, the rotational correlation time and the outer splitting values are very close to those of the BSA and BSA+TiO2 samples, whereas the filtered BSA has negligible immobile component (but with smaller outer splitting, similarly to 5-SASL). It should be noted that the rotational correlation times are at the fast limit of the EPR time window for spin labels [54,67]. These values most probably correspond to free rotation of the spin label in water (5-MSL is much smaller than 5-SASL). The ~4 times reduced fraction of the immobile component in the filtered sample is likely to be related to the ~4 times lower concentration of BSA in the filtered sample than in BSA and BSA+TiO2 samples. Variation in τR is likely to be caused by colliding of the unbound label with the surface of slow-tumpling BSA (reducing the mean τR), which is in agreement with the observation that τR is smaller in the filtered BSA sample, in which the BSA concentration is smaller than in the other two BSA-containing samples. A similar explanation applies when comparing 5-MSL in water vs. in the BSA samples. It should be also noted that the outer splitting (hence the orientational disorder) are comparable to those obtained with 5-SASL.

2.4.3. Spin-labelling with MTSL

Spin-labelling with MTSL was done in the same way as with 5-MSL. MTSL (Figure 4C) has a disulphide bridge between the doxyl ring and the free sulfhydryl group of the Cysteine amino acid, which gives more rotational freedom and flexibility for this label compared with 5-MSL. It is therefore expected that MTSL displays higher mobility than 5-MSL. The EPR spectra of MTSL in water and the BSA-containing samples are shown in Figure 7.

Preprints (www.preprints.org) | NOT PEER-REVIEWED | Posted: 15 August 2023 doi:10.20944/preprints202308.1111.v1

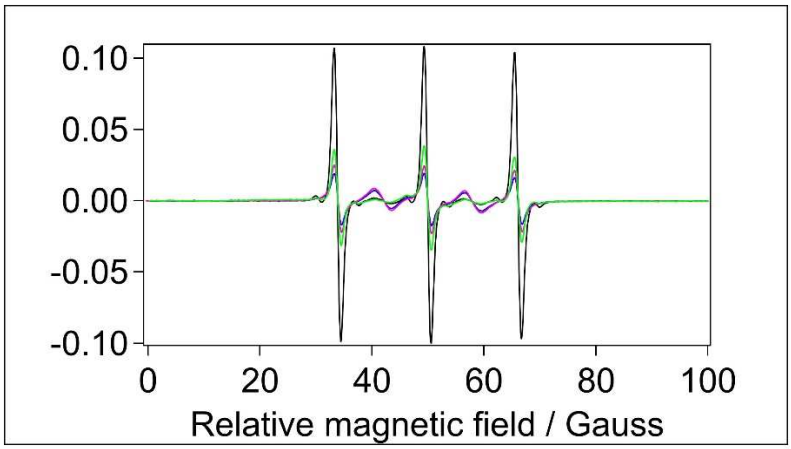

Figure 7. Normalised CW EPR spectra of samples labelled with MTSL. Black: water, blue: BSA in water, magenta: filtered BSA, green: BSA+TiO_2, [MTSL]=1.2x10^{-4} M.

Through optimised spectral subtractions, we found that the MTSL spectra have three components: in addition to the expected mobile and an immobile components we observed a 5-peak component known to originate from the dimeric (biradical) form of this type of label [68]. Fortunately, the five peaks of the dimeric form do not overlap with the three lines of the immobile component of the normal, monomeric form. Therefore, using diluted samples to change the contribution of 5-peak component (not shown), the three components could be separated. Although we see an immobile component observed earlier [31], it is almost undetectable, hence the outer splittings could not be determined. Table 6. reports the fractional contribution of the mobile and immobile component and the rotational correlation time derived from the mobile component of monomeric MTSL in water and in the BSA-containing samples.

Table 6. EPR parameters of samples spin-labelled with MTSL. [MTSL]=1.2x10^{-4} M.

Sample	Mobile component/%	Immobile component/%	τ/ns	$2A_{zz}$/G
water	-	0.009378	-	100
BSA	-	0.04578	2-3	97-98
Filtered BSA	-	0.04237	-	100
BSA+TiO2	-	0.05361	2-3	97-98

According to its mobile component, the rotation of the monomeric MTSL is ~5-6 times slower in the BSA-containing samples than in water, and ~5-8 times slower than 5-MSL in the corresponding samples. We can not exclude that mobile components are from bound MTSL but it is more likely that this label did not bind to the protein and the mobile component is from MTSL monomers in water, and the effective rotational correlation time is increased in BSA-containing samples by diffusional collisions with the protein micelles, which is confirmed by the apparent concentration dependence of τR in the dilution experiment (not shown). Nevertheless, the rotation correlation times showed the same tendency as in the case of spin-labelling with 5-MSL (Table 6).

3. Materials and Methods

3.1. Chemicals, sample preparation

Bovine Serum Albumin (BSA) and TiO_2 Aeroxide P25 were of analytical grade and purchased from VWR International (Hungary). Pristine and modified Polyvinylidene fluoride (PVDF) with molecular weight cut off (MWCO) values of 100 kDa ultrafilter (UF) membranes Kynar 400 PVDF 100 kDa molecular weight cut off (MWCO) were purchased from New Logic Research Inc., USA. The spin labels, 5-doxyl stearic acid (5-SASL) and 3-maleimido-proxyl (5-MSL) were purchased from

 doi:10.20944/preprints202308.1111.v1

Sigma and 1-(oxyl-2,2,5,5-tetramethylpyrrolidine-3-methyl) methanethiosulfonate (MTSL) was from Santa Cruz Biotechnology (USA). Ethanol was from Molar Chemicals.

The ultrafilter membranes were prepared by coating PVDF with inorganic TiO_2 nanoparticles. Commercial PVDF membranes were used to prepare nanoparticles-coated membranes by a physical deposition method [4]. For this purpose, 0.04 g of commercial TiO_2 was added to 100 mL of ultrapure water and ultrasonicated for 3 min. Then, the ultrasonicated suspension was filtered through a membrane in a dead-end filtration device (Millipore, XFUF04701, Merck KGa, Darmstadt, Germany) at 0.3 MPa and dried for 1 h at room temperature before use. The procedure of the filtration has been done as described previously [4]. Briefly, BSA rejection tests were performed at 0.1 MPa. In each filtration, 250 mL of water or model solution was filtered until gaining a 200 mL of permeate. Concentration of BSA was measured before and after filtration by measuring chemical oxygen demand (COD) of the solution and BSA rejection was calculated. To check the potential effect of TiO_2 nanoparticles on BSA filtration performance, another sample was prepared as follows: 0.04 g TiO_2 and 250 mg BSA were dissolved in 250 ml ultrapure water and stirred (350 rpm) for 1.5 h, then filtered through a 0.22 μm Cellulose acetate (CA) syringe filter to separate BSA from TiO_2. The clear BSA solution was then filtered through the unmodified PVDF ultrafilter membrane (labelled as BSA/TiO_2@PVDF), and COD rejection was calculated. Rejection was calculated using the following equation:

$$R(\%) = \frac{C_0 - C}{C_0} \times 100 \quad (3)$$

where C_0 and C are the concentrations of feed and permeate solutions, respectively.

In order to examine the potential effect of TiO_2 on BSA, four types of samples were analysed with EPR and fluorescent spectroscopy: (1) BSA 4 g/l in water, (2) TiO_2 1.6 g/l in water, (3) BSA-TiO_2 mixture where BSA 4 g/l and TiO_2 1.6 g/l in water and (4) BSA 4g/l filtered through composite ultrafilter membranes.

The spin labels were dissolved in ethanol (6 mM) for the stock solutions. Protein concentration was checked by Lowry method [69]. The BSA concentration was always reduced by the filtration, concentrations for filtered BSA stocks were determined to be typically ~1.2 g/l. However, the protein concentration in the (un-filtered) BSA and BSA+TiO_2 samples were not adjusted to that of filtered ones because we wanted to avoid any change in the original samples.

3.2. Experimental procedures and data analysis

COD was measured by the standard potassium-dichromate oxidation method using standard test tubes (Lovibond) and digestion and COD measurements were carried out in a COD digester (Lovibond, ET 108) and a COD photometer (Lovibond PC-CheckIt).

Dynamic Light Scattering measurements for BSA were made by a Zetasizer Nano ZS, Malvern (UK) instrument. The principle of the DLS technique is that fine particles and molecules that are in Brownian motion, diffuse at a speed related to their size. To measure the diffusion speed, the scattered light of a He-Ne laser (633 nm) illuminating the particles is recorded. The light intensity at a specific angle fluctuates with time, which is recorded using a sensitive avalanche photodiode detector. The autocorrelation function of this time-series curve is informative to the size distribution of the hydrodynamic radius of the particles [70]. The samples contained 0.002, 0.02, 0.04 and 4 g/l BSA in water.

Fluorescence measurements were carried out by a Fluorolog-3 (FL3-222) modular spectrofluorimeter (Horiba (Jobin Yvon), Japan) with the excitation wavelength of 295 nm. Stocks and 30 times diluted solutions of BSA, BSA+TiO_2 and filtered BSA were used for the measurements.

Continuous wave EPR measurements were carried out on a Bruker ELEXSYS-II E580 X-band spectrometer at room temperature, with the following instrument settings: scan range 3300-3400 G, microwave frequency ~ 9.42 GHz; microwave power 9.464 mW, modulation frequency 100 kHz, modulation amplitudo 0.4 G, resolution of field axes 1024, to scans, 16, sweep time 40.96 s. The first series of experiments had the molar ratio of protein and spin labels 1:2 where the concentration of the spin label was 1.2×10^{-4} M with the volume ratio of 2%. Further sample series were 5- or 10-fold diluted either for both the stocks and the spin labels, hence preserving all the molar ratios or only those for the spin labels.

Data analysis, fitting the plotting were done with *Igor Pro*, version 8.02 (Wave Metrics, Lake Oswego, Oregon 97035, USA). Molecular graphics was made with *YASARA,* version 21.12.19 [71].

4. Conclusions

Although filtering causes ~4-fold reduction in the BSA concentration, it is still way above the CMC. Therefore the observed effects, reported by EPR and fluorescence spectroscopy, are not caused by changes in the particle sizes. Small protein oligomers represent a negligible phase of BSA as opposed to the large micelles or oligomers present in all the samples over a wide size distribution. These large particles represent low mobility in the EPR time scale, which is reflected by the immobile component of the EPR spectra of tightly bound fraction of spin labels (5-SASL and 5-MSL). The potentially more loosely bound MTSL has negligible bound fraction. It is important to note that the source of fluorescence signal and the EPR of spin-labelled fatty acids are not as specific as the EPR of the uniquely un-blocked Cys34, since there are two Trp residues and up to 7 fatty acid binding pockets in BSA. Indeed, there are indications that all binding sites in an albumin may be have bound fatty acid even at the lowest levels of ligand loading [31]. In addition, Cys34 (in domain I) is relatively close to the protein surface [64,65], and when spin-labelled, it has been reported to be more accessible to collisional interaction with water-soluble paramagnetic relaxant than the acyl chain of non-covalently bound spin-labelled fatty acids (located in hydrophobic channels in the protein) [28]. The Trp region is more sensitive to prolonged effect of TiO_2 nanoparticles, whereas both the stearic acid binding pocket and the environment of spin-labelled Cysteine are more sensitive to the mechanical stress caused by the filtration process. The difference between these processes (as compared to BSA dissolved in water) is that filtration exerts a mechanical stress on the protein and its aggregated forms (micelles) with a relatively short duration of contact with TiO_2. On the contrary, mixing with TiO_2 lacks a mechanical stress to BSA but the protein is exposed to interaction with TiO_2 for a long period of time. The visual appearance of the BSA solutions suggested that there is no precipitation of BSA and the spectroscopic data support that BSA remained in a folded conformation throughout the experiments.

It can be concluded that the filtration process and prolonged exposure to TiO_2 have significant effect on different regions of BSA. However, of denaturing the protein by the TiO_2 covered surface of the filter membrane was not observed. Obviously, further research is needed, for instance, in the direction of slower filtering and/or different coating materials with higher elimination efficiency.

Author Contribution: K.S-N. made the EPR experiments and helped interpreting the data and drafting the manuscript. Z.K. made the fluorescence experiments. A.K. made, A.D. evaluated and interpreted the DLS experiments. A.F.F made the COD experiments. Z.L. proposed the project, supervised the COD experiments, provided the membrane filters and TiO2 nanoparticles and contributed to the interpretation of the results. T.P. coordinated the work, designed the spectroscopy experiments and interpreted the results, provided the concept of the manuscript and refined it to its final form. All authors have read and agreed to the published version of the manuscript.

Data Availability Statement: All experimental data presented in this study are available on request from the corresponding author.

Acknowledgments: This research was funded in part by the National Research, Development and Innovation Office of Hungary-PD-143268.

Conflicts of Interest: The authors declare no conflict of interest. There was not any external influence on the authors in the design of the study; in the collection, analyses, or interpretation of data; in the writing of the manuscript; or in the decision to publish the results.

References

1. Wangoo, N; Suri, C.R.; Shekhawat, G. Interaction of Gold Nanoparticles with Protein: A Spectroscopic Study to Monitor Protein Conformational Changes. *Appl Phys Lett*, **2008**, *92*, 133104., https://doi.org/10.1063/1.2902302
2. Gheshlaghi, ZN; Riazi ,G.H.; Ahmadian, S.; Ghafari, M.; Mahinpour, R. Toxicity and Interaction of Titanium Dioxide Nanoparticles with Microtubule Protein. *Acta Biochim Biophys Sin*, **2008**, *40*, 777–782., PMID: 18776989.

3. Bardhan, M.; Mandal, G.; Ganguly, T. Steady State, Time Resolved, and Circular Dichroism Spectroscopic Studies to Reveal the Nature of Interactions of Zinc Oxide Nanoparticles with Transport Protein Bovine Serum Albumin and to Monitor the Possible Protein Conformational Changes. *J Appl Phys*, **2009**, *106*, 034701., https://doi.org/10.1063/1.3190483
4. Jigar, E.; Bagi, K.; Fazekas, Á.; Kertész, S.; Veréb, G.; László, Z. Filtration of BSA through TiO2 Photocatalyst Modified PVDF Membranes. *Desalin Water Treat*, **2020**, 192392-192399., https://doi.org/10.5004/dwt.2020.25464
5. Sisay, E.J.; Fazekas, Á.F.; Gyulavári, T.; Kopniczky, J.; Hopp, B.; Veréb, G. et al. Investigation of Photocatalytic PVDF Membranes Containing Inorganic Nanoparticles for Model Dairy Wastewater Treatment. *Membranes*, **2023**, *13(7)*, 656., https://doi.org/10.3390/membranes13070656
6. Saptarshi, S.R.; Duschl, A.; Lopata. A.L. Interaction of Nanoparticles with Proteins: Relation to Bio-Reactivity of the Nanoparticle. *J Nanobiotechnology*, **2013**, *11(1)*, 26., https://doi.org/10.1186/1477-3155-11-26
7. Cao, X.; Ma, J.; Shi, X.; Ren, Z. Effect of TiO 2 Nanoparticle Size on the Performance of PVDF Membrane. *Appl Surf Sci*, **2006**, *253(4)*, 2003-2010., https://doi.org/10.1016/j.apsusc.2006.03.090
8. Liu, C.; Guo, Y.; Hong, Q.; Rao, C.; Zhang, H.; Dong, Y. et al. Bovine Serum Albumin Adsorption in .Mesoporous Titanium Dioxide: Pore Size and Pore Chemistry Effect. *Langmuir*, **2016**, *32(16)*, 3995-4003., https://doi.org/20.10.1021/acs.langmuir.5b04496
9. Wang, X.; Zhou, M.; Meng, X.; Wang, L.; Huang, D. Effect of Protein on PVDF Ultrafiltration Membrane Fouling Behavior under Different pH Conditions: Interface Adhesion Force and XDLVO Theory Analysis. *Front Environ Sci Eng*, **2016**, *10(4)*, 12., https://doi.org/10.1007/s11783-016-0855-9
10. Márquez, A.; Berger, T.; Feinle, A.; Hüsing, N.; Himly, M.; Duschl, A. et al. Bovine Serum Albumin Adsorption on TiO2 Colloids: The Effect of Particle Agglomeration and Surface Composition. *Langmuir*, **2017**, *33(10)*, 2551-2558., https://doi.org/10.1021/acs.langmuir.6b03785
11. Shen, L.; Feng, S.; Li, J.; Chen, J.; Li, F.; Lin, H. et al. Surface Modification of Polyvinylidene Fluoride (PVDF) Membrane via Radiation Grafting: Novel Mechanisms Underlying the Interesting Enhanced Membrane Performance. *Sci Rep*, **2017**, *7(1)*, 2721., https://doi.org/10.1038/s41598-017-02605-3
12. Nascimben Santos, E.; Fazekas, Á.; Hodúr, C.; László, Z.; Beszédes, S.; Scheres Firak, D. et al. Statistical Analysis of Synthesis Parameters to Fabricate PVDF/PVP/TiO2 Membranes via Phase-Inversion with Enhanced Filtration Performance and Photocatalytic Properties. *Polymers (Basel)*, **2021**, *14(1)*, 113., https://doi.org/10.3390/polym14010113
13. Squire, P.G.; Moser, P.; O'Konski, C. T. The Hydrodynamic Properties of Bovine Serum Albumin Monomer and Dimer. *Biochemistry*, **1968**, *7(12)*, 4261-4272., https://doi.org/10.1021/bi00852a018
14. Brahma, A.; Mandal, C.; Bhattacharyya, D. Characterization of a Dimeric Unfolding Intermediate of Bovine Serum Albumin under Mildly Acidic Condition. *Biochim Biophys Acta*, **2005**, *1751(2)*, 159-169., https://doi.org/10.1016/j.bbapap.2005.06.007
15. Masuelli, M.A. Study of Bovine Serum Albumin Solubility in Aqueous Solutions by Intrinsic Viscosity Measurements. *Adv Phys Chem*, **2013**, 20131-20138., https://doi.org/10.1155/2013/360239
16. Devi, L.B.; Mandal, *A.B.* BSA can Form Micelle in Aqueous Solution. *J Surface Sci Technol*, **2015**, *31*, 21-29., https://doi.org/10.18311/jsst/2015/1699
17. Li, R.; Wu, Z.; Wangb, Y.; Ding, L.; Wang, Y. Role of pH-Induced Structural Change in Protein Aggregation in Foam Fractionation of Bovine Serum Albumin. *Biotechnol Rep (Amst)*, **2016**, *9*, 46-52., 10.1016/j.btre.2016.01.002
18. Varga, N.; Hornok, V.; Sebők, D.; Dékány, I. Comprehensive Study on the Structure of the BSA from Extended-to Aged Form in Wide (2-12) pH Range. *Int J Biol Macromol*, **2016**, *88*, 51-58., https://doi.org/10.1016/j.ijbiomac.2016.03.030
19. de Sousa Neto, D.; Salmon, C.E.; Alonso, A.; Tabak, M. Interaction of Bovine Serum Albumin (BSA) with Ionic Surfactants Evaluated by Electron Paramagnetic Resonance (EPR) Spectroscopy. *Colloids Surf B Biointerfaces*, **2009**, *70(1)*, 147-156., https://doi.org/10.1016/j.colsurfb.2008.12.026
20. Neacsu, M-V.; Matei, I.; Ionita, G. The Extent of Albumin Denaturation Induced by Aliphatic Alcohols: an Epr and Circular Dichroism Study. *Rev Roum Chim*, **2017**, *62(8-9)*, 637-643.
21. Pavićević, A.; Luo, J.; Popović-Bijelić, A.; Mojović, M. Maleimido-proxyl as an EPR Spin Label for the Evaluation of Conformational Changes of Albumin. *Eur Biophys J*, **2017**, *46(8)*, 773-787., https://doi.org/10.1007/s00249-017-1257-z
22. Reichenwallner, J.; Oehmichen, M.-T.; Schmelzer, C.; Hauenschild, T.; Kerth, A.; & Hinderberger, D. Exploring the pH-Induced Functional Phase Space of Human Serum Albumin by EPR Spectroscopy. *Magnetochemistry*, **2018**, *4*, 47., 10.3390/magnetochemistry4040047
23. Spector, A.A.; John, K.; Fletcher, J.E. Binding of Long-chain Fatty Acids to Bovine Serum Albumin. *J Lipid Res*, **1969**, *10(1)*, 56-67.
24. Simard, J.R.; Zunszain, P.A.; Hamilton, J.A.; Curry, S. Location of High and Low Affinity Fatty Acid Binding Sites on Human Serum Albumin Revealed by NMR Drug-competition Analysis. *J Mol Biol*, **2006**, *361(2)*, 336-351., https://doi.org/10.1016/j.jmb.2006.06.028

25. Fanali, G.; di Masi, A.; Trezza, V.; Marino, M.; Fasano, M.; Ascenzi, P. Human Serum Albumin: from Bench to Bedside. *Mol Aspects Med*, **2012**, *33(3)*, 209-290., https://doi.org/10.1016/j.mam.2011.12.002
26. Rizzuti, B.; Bartucci, R.; Sportelli, L.; Guzzi, R. Fatty Acid Binding into the Highest Affinity Site of Human Serum Albumin Observed in Molecular Dynamics Simulation. *Arch Biochem Biophys*, **2015**, *579*, 18-25., https://doi.org/10.1016/j.abb.2015.05.018
27. Ge, M.T.; Rananavare, S.B.; Freed, J.H. ESR Studies of Stearic Acid Binding to Bovine Serum Albumin. *Biochim Biophys Acta*, **1990**, *1036(3)*, 228-236., https://doi.org/10.1016/0304-4165(90)90039-y
28. Livshits, V. A. Marsh, D. Fatty Acid Binding Sites of Serum Albumin Probed by Non-linear Spin-label EPR. *Biochim Biophys Acta*, **2000**, *1466(1-2)*, 350-360., 10.1016/s0005-2736(00)00194-2
29. Junk, M.J.; Spiess, H.W.; Hinderberger, D. DEER in Biological Multispin-systems: a Case Study on the Fatty Acid Binding to Human Serum Albumin. *J Magn Reson*, **2011**, *210(2)*, 210-217., https://doi.org/10.1016/j.jmr.2011.03.003
30. Pavićević, A.A.; Popović-Bijelić, A.D.; Mojović, M.D.; Šušnjar, S.V.; Bačić, G.G. Binding of Doxyl Stearic Spin Labels to Human Serum Albumin: an EPR Study. *J Phys Chem B*, **2014**, *118(37)*, 10898-10905., 10.1021/jp5068928
31. Reichenwallner, J.; Hauenschild, T.; Schmelzer, C.E.H.; Hülsmann, M.; Godt, A.; Hinderberger, D. Fatty Acid Triangulation in Albumins Using a Landmark Spin Label. *Isr J Chem*, **2019**, *59(11-12)*, 1059-1074., https://doi.org/10.1002/ijch.201900073
32. Morrisett, J. D.; Pownall, H.J.; Gotto, A.M. Bovine serum albumin. Study of the Fatty Acid and Steroid Binding Sites using Spin-labeled lipids. *J Biol Chem*, **1975**, *250(7)*, 2487-2494., PMID: 164444.
33. Perkins, R.C.; Abumrad, N.; Balasubramanian, K.; Dalton, L.R.; Beth, A.H.; Park, J.H. et al. Equilibrium Binding of Spin-labeled Fatty Acids to Bovine Serum Albumin: Suitability as Surrogate Ligands for Natural Fatty Acids. *Biochemistry*, **1982**, *21(17)*, 4059-4064., 10.1021/bi00260a023
34. Benga, G.; Strach, S.J. Interpretation of the Electron Spin Resonance Spectra of Nitroxide-maleimide-labelled Proteins and the Use of this Technique in the Study of Albumin and Biomembranes. *Biochim Biophys Acta*, **1975**, *400(1)*, 69-79., https://doi.org/10.1016/0005-2795(75)90127-0
35. Marsh, D.; Livshits, V.A.; Pali, T.; Gaffney, B.J. Recent Development in Biological Spin-label Spectroscopy. In *Spectroscopy of Biological Molecules: New Directions*, Greve, J., Puppels, G.J., Otto, C., Eds.; Dordrecht, Boston, London: Kluwer Academic Publishers. 1999; pp. 647-650., 10.1007/978-94-011-4479-7_291
36. Páli, T.; Marsh, D. Structural Studies on Membrane Proteins Using Non-linear Spin Label EPR Spectroscopy. *Cell Mol Biol Lett*, **2002**, *7(1)*, 87-91., PMID: 11944054
37. Bordignon, E. EPR Spectroscopy of Nitroxide Spin Probes. E*MagRes*, **2017**, 6235-6254., https://doi.org/10.1002/9780470034590.emrstm1513
38. Bujacz, A. Structures of Bovine, Equine and Leporine Serum Albumin. *Acta Crystallogr D Biol Crystallogr*, **2012**, *68*, 1278-1289., https://doi.org/10.1107/S0907444912027047
39. The UniProt Consortium. UniProt: the Universal Protein Knowledgebase in 2023. *Nucleic Acids Res*, **2023**, *51(D1)*, D523–D531., https://doi.org/10.1093/nar/gkac1052
40. https://doi.org/10.2210/pdb4F5S/pdb
41. Celej, M.S.; Montich, G.G.; Fidelio, G.D. Protein Stability Induced by Ligand Binding Correlates with Changes in Protein Flexibility. *Protein Sci*, **2003**, *12(7)*, 1496-1506., https://doi.org/10.1110/ps.0240003
42. Togashi, D.M; Ryder, A.G.; Mc Mahon, D.; Dunne, P.; McManus, J. Fluorescence Study of Bovine Serum Albumin and Ti and Sn Oxide Nanoparticles Interactions. in *Diagnostic Optical Spectroscopy in Biomedicine IV*, Schweitzer, D.; Fitzmaurice, M., Eds., Optica Publishing Group,Vol. 6628 of Proceedings of SPIE-OSA Biomedical Optics, 2007; paper 6628_61, https://doi.org/10.1364/ECBO.2007.6628_61
43. Bhattacharya, M.; Jain, N.; Bhasne, K.; Kumari, V.; Mukhopadhyay, S. pH-Induced Conformational Isomerization of Bovine Serum Albumin Studied by Extrinsic and Intrinsic Protein Fluorescence. *J Fluoresc*, **2011**, *21(3)*, 1083-1090., https://doi.org/10.1007/s10895-010-0781-3
44. Vivian, J.T.; Callis, P.R. Mechanisms of Tryptophan Fluorescence Shifts in Proteins. *Biophys J*, **2001**, *80(5)*, 2093-2109., https://doi.org/10.1016/S0006-3495(01)76183-8
45. Dos Santos Rodrigues, F.H.; Delgado, G.G.; Santana da Costa, T.; Tasic, L. Applications of Fluorescence Spectroscopy in Protein Conformational Changes and Intermolecular Contacts. *BBA Adv*, **2023**, *3*, 100091., https://doi.org/10.1016/j.bbadva.2023.100091
46. Li, Y.; Yang, G.; Mei, Z. Spectroscopic and Dynamic Light Scattering Studies of the Interaction between Pterodontic Acid and Bovine Serum Albumin. *Acta Pharm Sin B*, **2012**, 2(1), 53-59., https://doi.org/10.1016/j.apsb.2011.12.001
47. Polat, H.; Kutluay, G.; Polat, M. Analysis of Dilution Induced Disintegration of Micellar Drug Carriers in the Presence of Inter and Intra Micellar Species. *Colloids and Surfaces A*, **2020**, *601*, 124989., https://doi.org/10.1016/j.colsurfa.2020.124989
48. Burgstaller, C.; N. Etchart, N. Dimerization of Bovine Serum Albumin as Evidenced by Particle Size and Molecular Mass Measurement. Anton Paar GmbH. D51 | A044EN-A, Available online: https://s3-eu-central-

1.amazonaws.com/centaur-wp/theengineer/prod/content/uploads/2018/04/05161827/Bovine-serum-albumin-testing.pdf (2018)
49. Howe, K.J; Clark, M.M. Fouling of Microfiltration and Ultrafiltration Membranes by Natural Waters. *Environ Sci Technol*, **2002**, *36*, 3571–3576., https://doi.org/10.1021/es025587r
50. Bacova, J.; Knotek, P.; Kopecka, K.; Hromádko, L.; Čapek, J.; Nývltová, P.; Bruckova, L.; Schroterova, L.; Sestakova, B.; Palarcik, J.; Motola, M. Cízková, D.; Bezrouk, A.; Handl, J.; Fiala, Z.; Rudolf, E.; Bílková, Z.; Macak, J.; Rousar, T. Evaluating the Use of TiO2 Nanoparticles for Toxicity Testing in Pulmonary A549 Cells. *Int J Nanomed*, **2022**, *17*, 4211-4225, https://doi.org/10.2147/IJN.S374955
51. Teale, F.W.J.; Weber, G. Ultraviolet Fluorescence of the Aromatic Amino Acids. *Biochem J*. **1957**, *65(3)*, 476–482., https://doi.org/10.1042/bj0650476
52. Pocanschi, C.L.; Popot, J.L.; Kleinschmidt, J.H. Folding and Stability of Outer Membrane Protein A (OmpA) from Escherichia Coli in an Amphipathic Polymer, Amphipol A8-35. *Eur Biophys J*, **2013**, *42(2-3)*, 103-118., https://doi.org/10.1007/s00249-013-0887-z
53. Koch, D.; Manzhos, S. On the Charge State of Titanium in Titanium Dioxide. *J Phys Chem Lett*, **2017**, *8*, 1593−1598., https://doi.org/10.1021/acs.jpclett.7b00313
54. Freed, J.H. Theory of Slow Tumbling ESR Spectra of Nitroxides. In *spin labeling. Theory and Applications*, Berliner, L.J., Ed.; New York: Academic Press. 1976; pp. 53-132.
55. Hubbell, W.L.; Lopez, C.J.; Altenbach, C.; Yang, Z. Technological Advances in Site-directed Spin Labeling of Proteins. *Curr Opin Struct Biol*, **2013**, *23(5)*, 725-733., https://doi.org/10.1016/j.sbi.2013.06.008
56. Lopez, C.J.; Fleissner, M.R.; Brooks, E. K.; Hubbell, W. L. Stationary-phase EPR for Exploring Protein Structure, Conformation, and Dynamics in Spin-labeled Proteins. *Biochemistry*, **2014**, *53(45)*, 7067-7075., https://doi.org/10.1021/bi5011128
57. Marsh, D. Spin-label Order Parameter Calibrations for Slow Motion. *Appl Magn Reson*, **2018**, *49(1)*, 97-106., https://doi.org/10.1007/s00723-017-0940-7
58. Páli, T.; Kóta, Z. Studying Lipid-Protein Interactions with Electron Paramagnetic Resonance Spectroscopy of Spin-labeled Lipids. *Methods Mol Biol*, **2019**, 2013529-561., https://doi.org/10.1007/978-1-4939-9512-7_22
59. Kivelson, D. Theory of ESR Linewidths of Free Radicals. *J Chem Phys*, **1960**, *33*, 1094-1107., 10.1063/1.1731340
60. Páli T.; Pesti M.; Chapter V: Phase Transition of Membrane Lipids. In *Manual on Membrane Lipids*, Prasad, R., Ed.; Berlin, Heidelberg, New York: Springer-Verlag. 1996; pp. 80-111., https://doi.org/10.1007/978-3-642-79837-5_5
61. Griffith, O.H.; Jost, P.C. Lipid Spin Labels in Biological Membranes. *In Spin Labeling. Theory and Applications*, L. J. Berliner Ed.; New York: Academic Press. 1976; pp. 453-523., https://doi.org/10.1007/978-1-4613-0743-3
62. Peters Jr., T. Ligand Binding in Albumin In *All about Albumin*, Academic Press, 1995; pp. 76-132. https://doi.org/10.1016/B978-0-12-552110-9.X5000-4
63. Hull, H.H.; Raymond Chang, Lawrence J. Kaplan, On the Location of the Sulfhydryl Group in Bovine Plasma Albumin, *Biochim Biophys Acta*, **1975**, *400(1)*, 132-136., https://doi.org/10.1016/0005-2795(75)90133-6
64. Sugio, S.; Kashima, A.; Mochizuki, S.; Noda, M.; Kobayashi, K. Crystal Structure of Human Serum Albumin at 2.5 A Resolution. *Protein Eng*, **1999**, *12(6)*, 439-446., https://doi.org/10.1093/protein/12.6.439
65. Stewart, A.J.; Blindauer, C.A.; Berezenko, S.; Sleep, D.; Tooth, D.; Sadler, P.J. Role of Tyr84 in Controlling the Reactivity of Cys34 of Human Albumin. *FEBS J*, **2005**, *272(2)*, 353-362., https://doi.org/10.1111/j.1742-4658.2004.04474.x
66. Griffith, O.H.; McConnell, H.M. A Nitroxide-maleimide Spin Label. *Proc Natl Acad Sci U S A*, **1966**, *55(1)*, 8-11., https://doi.org/10.1073/pnas.55.1.8
67. Lange, A.; Marsh, D.; Wassmer, K. H.; Meier, P.; Kothe, G. Electron Spin Resonance Study of Phospholipid Membranes Employing a Comprehensive Line-Shape Model. *Biochemistry*, **1985**, *24*, 4383-4392., https://doi.org/10.1021/bi00337a020
68. Eaton, S.S.; Woodcock, L.B.; Eaton, G.R. Continuous Wave Electron Paramagnetic Resonance of Nitroxide Biradicals in Fluid Solution. *Concepts Magn Reson Part A*, **2018**, *47A(2)*, 21426., https://doi.org/10.1002/cmr.a.21426
69. Lowry, O.H.; Rosebrough, N.J.; Farr, L.; Randall, R.J. Protein Measurement with the Folin Phenol Reagent. *J Biol Chem*, **1951**, *193*, 265–275., PMID: 14907713
70. Taneva, S.G.; Krumova, S.; Bogár, F.; Kincses, A.; Stoichev, S.; Todinova, S.; Avgustina Danailova, Horváth, J.; Násztor, Z.; Kelemen, L.; Dér, A. Insights into Graphene Oxide Interaction with Human Serum Albumin in Isolated State and in Blood Plasma. *Int J Biol Macromol*, **2021**, *175*, 19-29., https://doi.org/10.1016/j.ijbiomac.2021.01.151
71. Krieger, E.; Vriend, G. YASARA View - Molecular Graphics for All Devices - from Smartphones to Workstations. *Bioinform*, **2014**, *30(20)*, 2981-2982., https://doi.org/10.1093/bioinformatics/btu426